https://doi.org/10.5194/angeo-2024-25
Preprint. Discussion started: 20 November 2024

Annales Geophysicae Discussions

"Study of Temperature Anisotropy and Kappa Distribution Impacts on EMIC Waves in Multi-Species Magnetized Plasma"

Rahul Bhaisaniya[1] *and Ganpat Ahirwar*[2]
[1]*Assistant Professor,Govt PG college Rajgarh, MP,India*
[2]*Assistant Professor ,School of Studies in Physics,Vikram University Ujjain (M.P.)India*
[1]*EMail :rahulbhaisaniya@gmail.com*
[2]*EMail :ganpat.physics@gmail.com*
**Corresponding to: RAHUL BHAISANIYA , [1]EMail :rahulbhaisaniya@gmail.com*

Abstract:- This research investigates the impact of temperature anisotropy on Electromagnetic ion cyclotron (EMIC) waves in a multi-ion magneto-plasma environment composed of H^+, He^+, and O^+ ions, with a particular emphasis on the role of the Kappa distribution function. The study delves into how variations in temperature anisotropy influence the behavior and properties of EMIC wave propagation, considering the complex interplay between anisotropic thermal effects and the non-Maxwellian Kappa distribution. Through a comprehensive analysis involving theoretical modeling and numerical simulations, the research elucidates how these factors alter wave dispersion relations, growth rates, and spatial structures of EMIC waves. The results reveal significant deviations from classical Maxwellian predictions, highlighting the necessity to incorporate Kappa distributions for accurate descriptions of wave behavior in realistic plasma conditions. This enhanced understanding has broader implications for space physics, astrophysical phenomena, and laboratory plasma experiments, where non-equilibrium conditions and multiple ion species are prevalent. The results are analyzed in the context of space plasma parameters relevant region within Earth's magnetosphere..

Introduction

Electromagnetic ion cyclotron (EMIC) waves are transverse, low frequency (below the proton cyclotron frequency) waves in the range of 0.1-5Hz are seen on the ground as pc1-pc2 pulsations. Electromagnetic ion cyclotron waves generated in In the equatorial region of Earth's magnetosphere, left-handed circularly polarized waves propagate along magnetic field lines, guided towards the ionosphere15. Experiment evidence for naturally occurring ion cyclotron instability has been summarized by Cornwall. The auroral acceleration region present about the earth at magnetic latitudes of about ±70 and at altitude between a typically above 4000km. In this region, large amplitude electric field structure has been observed . According to Yan et

https://doi.org/10.5194/angeo-2024-25
Preprint. Discussion started: 20 November 2024

al., the auroral acceleration region can be approximated as a low β, cold plasma environment. The parallel electric fields are generally observed to be concentrated around 6000 km altitude, a zone known as the auroral acceleration region. Although the exact nature of parallel electric fields remains debated, most researchers link them to the field-aligned currents present in the auroral region24.

Electromagnetic ion cyclotron (EMIC) waves are significant in space plasma physics, particularly within the Earth's magnetosphere, where they influence particle dynamics, energy transfer, and overall plasma behaviour (Anderson & Williams, 1999; Kennel & Petschek, 1966). These waves propagate at frequencies near the ion cyclotron frequency and are crucial for understanding various plasma processes, including wave-particle interactions and the heating of ion populations (Chen & Hasegawa, 1974).

Traditionally, studies of EMIC waves have employed the Maxwellian distribution to describe particle velocities in plasmas. However, the Kappa distribution function, characterized by its parameter kappa, provides a more nuanced representation of particle velocity distributions, especially in environments where non-thermal or suprathermal particles are prevalent (Pierrard & Lazar, 2010). This distribution function better accommodates the high-energy tails observed in many astrophysical and space plasma contexts, making it a valuable tool for accurately modelling wave phenomena in these settings (Vasyliunas, 1968).

Temperature anisotropy, where the temperature varies along different spatial directions, further complicates the plasma environment. Anisotropic temperature conditions can significantly affect wave propagation, altering dispersion relations, growth rates, and wave stability (Hellinger & Matsumoto, 2000). For instance, in a magneto-plasma with anisotropic temperatures, the perpendicular and parallel temperatures relative to the magnetic field can lead to enhanced wave growth and modified dispersion characteristics compared to isotropic conditions (Zhang & Chen, 2003).

When combined with a Kappa distribution, the effects of temperature anisotropy introduce additional complexities. The interaction between the Kappa distribution and temperature anisotropy can lead to novel wave behaviors that deviate from those predicted by Maxwellian distributions alone (Del Sarto, Pegoraro, & D'Angelo, 2011; Scholer, 1988). This interaction can impact various plasma parameters, including wave amplitude, frequency, and spatial structure, thereby influencing the overall dynamics of the plasma system.

https://doi.org/10.5194/angeo-2024-25
Preprint. Discussion started: 20 November 2024

Despite the significance of these factors, the combined effects of temperature anisotropy and Kappa distribution on EMIC waves remain underexplored. Understanding these interactions is essential for improving theoretical models and practical applications in space and laboratory plasmas, where complex conditions often prevail. This study aims to bridge this gap by examining how temperature anisotropy affects EMIC wave characteristics in a multi-ion magneto-plasma environment under the influence of a Kappa distribution function. By integrating theoretical analysis with numerical simulations, this research seeks to provide a comprehensive understanding of wave dynamics in such complex plasma systems.

BASIC TRAJECTORIES

Consider the path of the particle in the presence of EMIC waves ,various properties are derived for different kappa distribution index (Rana et.al 2021)1.

Given that the wave travels along the z-axis in the specified direction of the magnetic field, the left-handed circularly polarized EMIC wave in a cold magnetized plasma with angular frequency ω is defined as follows

$$B_x = \cos(k_{\Pi l}\mathrm{z} - \omega \mathrm{t}) \tag{A}$$

$$B_y = \sin(k_{\Pi l}\mathrm{z} - \omega \mathrm{t}) \tag{B}$$

When the system moves with the wave, the electric field reduces to zero.

$$B = B_x \cos(k_{\Pi l}\mathrm{z})\, x + B_y \sin(k_{\Pi l}\mathrm{z})\, y \tag{C}$$

Where the following conditions apply

$$Z^{wave} = Z^{lab} - \left(\frac{\omega}{k_{\Pi l}}\right) t \tag{D}$$

$$V^{wave} = V^{lab} - \left(\frac{\omega}{k}\right) t \tag{E}$$

As $\frac{ck}{\omega} \gg 1$, As The magnetic field amplitude is considered identical. Thus, the equation of ion motion in the wave is given as

$$\frac{\boldsymbol{dv_l}}{\boldsymbol{dt}} = \frac{q_l}{m_l c}\left[(V_l \times B_O) + (V_l \times B)\right] \tag{1}$$

We use cylindrical coordinates in velocity space as follows

$$v_{lx} = V_{\perp l} \cos\phi \tag{2}$$

$$v_{ly} = V_{\perp l} \sin\phi \tag{3}$$

https://doi.org/10.5194/angeo-2024-25
Preprint. Discussion started: 20 November 2024

$$v_{\perp lz} = V_{\Pi l} \tag{4}$$

The equation of motion is written as

$$\frac{dV_{\perp l}}{dt} = -V_{\Pi l}\Omega_l \sin(k_{\Pi} z - \phi) \tag{5}$$

$$V_{\perp l} = V_{\Pi lo} + \delta V_{\perp l} \tag{6}$$

$$V_{\Pi l} = V_{\Pi lo} + \delta V_{\Pi l} \tag{7}$$

Where V $_{\Pi i}$ initial values at t=0, Substituting eq. (1) to (5) in eq. (6) and (7) we find the following equations of The alterations in multi-ion velocities in the context of an EMIC wave are provided as,

$$\delta V_{\perp l} = \frac{\left[h\Omega_{H^+}\left(V_{\Pi H^+} - \frac{\omega}{K_{\Pi}}\right)\right]}{\left[k_{\Pi}V_{\Pi H^+{}_o} - (\omega - \Omega_{H^+})\right]} \times \left[\cos(k_{\Pi l}z - \omega t - \Psi) - \varepsilon \cos(k_{\Pi l}z - \omega t - \Psi - \left(k_{\Pi l}V_{\Pi H^+{}_o} - (\omega - \Omega_{H^+})\right)t\right] + \frac{\left[h\Omega_{He^+}\left(V_{\Pi He^+} - \frac{\omega}{K_{\Pi}}\right)\right]}{\left[k_{\Pi}V_{\Pi He^+{}_o} - (\omega - \Omega_{He^+})\right]} \times \left[\cos(k_{\Pi l}z - \omega t - \Psi) - \varepsilon \cos(k_{\Pi l}z - \omega t - \Psi - \left(k_{\Pi l}V_{\Pi He^+{}_o} - (\omega - \Omega_{He^+})\right)t\right] + \frac{\left[h\Omega_{O^+}\left(V_{\Pi O^+} - \frac{\omega}{K_{\Pi}}\right)\right]}{\left[k_{\Pi}V_{\Pi O^+{}_o} - (\omega - \Omega_{O^+})\right]} \times \left[\cos(k_{\Pi l}z - \omega t - \Psi) - \varepsilon \cos(k_{\Pi l}z - \omega t - \Psi - \left(k_{\Pi l}V_{\Pi O^+{}_o} - (\omega - \Omega_{O^+})\right)t\right] \tag{8}$$

$$\delta V_{\Pi l} = \frac{-hV_{\perp o}\Omega_{H^+}}{\left[k_{\Pi}V_{\Pi H^+{}_o} - (\omega - \Omega_{H^+})\right]} \times \left[\cos(k_{\Pi}z - \omega t - \Psi) - \varepsilon \cos(k_{\Pi}z - \omega t - \Psi - \left(k_{\Pi}V_{\Pi H^+{}_o} - (\omega - \Omega_l)\right)t\right] + \frac{-hV_{\perp o}\Omega_{H^+}}{\left[k_{\Pi}V_{\Pi He^+{}_o} - (\omega - \Omega_{He^+})\right]} \times \left[\cos(k_{\Pi}z - \omega t - \Psi) - \varepsilon \cos(k_{\Pi}z - \omega t - \Psi - \left(k_{\Pi}V_{\Pi He^+{}_o} - (\omega - \Omega_l)\right)t\right] + \frac{-hV_{\perp o}\Omega_{O^+}}{\left[k_{\Pi}V_{\Pi O^+{}_o} - (\omega - \Omega_{O^+})\right]} \times \left[\cos(k_{\Pi}z - \omega t - \Psi) - \varepsilon \cos(k_{\Pi}z - \omega t - \Psi - \left(k_{\Pi}V_{\Pi O^+{}_o} - (\omega - \Omega_l)\right)t\right] \tag{9}$$

Where $z = z_0 + V_{\Pi}\, t$ and $\psi = \psi_0 - \omega t$ and where ε=0 for non-resonant particles and ε=1 for resonant particles $h = \frac{B}{B_0}$.where $l = H^+/He^+/O^+$.

DISTRIBUTION FUNCTION

To examine *r*esonant and *non-r*esonant energies, growth rates, and growth lengths, we apply a Kappa distribution function as an extension within a multi-ion magneto-plasma environment

https://doi.org/10.5194/angeo-2024-25
Preprint. Discussion started: 20 November 2024

Annales Geophysicae Discussions
Open Access EGU

$$F_k(V_l) = \frac{1}{\pi^{3/2}\, V^2_{\perp H^+} V^2_{\Pi H^+}} \frac{\Gamma(k_p+1)}{{k_p}^{3/2}\Gamma(k_p-1/2)} \times \left\{1 + \frac{V^2_{\Pi H^+}}{k_p V^2_{\perp H^+}} + \frac{V^2_{\perp H^+}}{k_p V^2_{T\perp H^+}}\right\}^{-k_p-1} +$$

$$\frac{1}{\pi^{3/2}\, V^2_{\perp He^+} V^2_{\Pi He^+}} \frac{\Gamma(k_p+1)}{{k_p}^{3/2}\Gamma(k_p-1/2)} \times \left\{1 + \frac{V^2_{\Pi He^+}}{k_p V^2_{\perp He^+}} + \frac{V^2_{\perp He^+}}{k_p V^2_{T\perp He^+}}\right\}^{-k_p-1} +$$

$$\frac{1}{\pi^{3/2}\, V^2_{\perp O^+} V^2_{\Pi O^+}} \frac{\Gamma(k_p+1)}{{k_p}^{3/2}\Gamma(k_p-1/2)} \times \left\{1 + \frac{V^2_{\Pi O^+}}{k_p V^2_{\perp O^+}} + \frac{V^2_{\perp O^+}}{k_p V^2_{T\perp O^+}}\right\}^{-k_p-1} \quad (10)$$

$l = H^+/He^+/O^+.$

k_p is the kappa distribution index

bi-kappa distribution is implemented as

$$F_k(V_{\Pi l}) = \frac{1}{\pi^{1/2}\, V^2_{T\Pi H^+}} \frac{\Gamma(k_p+1)}{{k_p}^{3/2}\Gamma(k_p-1/2)} \left\{1 + \frac{V^2_{\Pi H^+}(\omega-\Omega_{H^+})^2}{K_\Pi V^2_{T\Pi H^+}}\right\}^{-k_p-1} + \frac{1}{\pi^{1/2}\, V^2_{T\Pi He^+}} \frac{\Gamma(k_p+1)}{{k_p}^{3/2}\Gamma(k_p-1/2)} \times$$

$$\left\{1 + \frac{V^2_{\Pi He^+}(\omega-\Omega_{He^+})^2}{K_\Pi V^2_{T\Pi He^+}}\right\}^{-k_p-1} + \frac{1}{\pi^{1/2}\, V^2_{T\Pi O^+}} \frac{\Gamma(k_p+1)}{{k_p}^{3/2}\Gamma(k_p-1/2)} \times \left\{1 +\right.$$

$$\left.\frac{V^2_{\Pi O^+}(\omega-\Omega_{O^+})^2}{K_\Pi V^2_{T\Pi O^+}}\right\}^{-k_p-1} \quad (11)$$

In above equation$V^2_{T\perp l}$and $V^2_{T\Pi l}$ are thermal velocity.

$$V^2_{T\perp l} = \left[\frac{k_p-3/2}{k}\frac{2k_pT_{\perp H^+}}{m_{H^+}}\right] + \left[\frac{k_p-3/2}{k}\frac{2k_pT_{\perp He^+}}{m_{He^+}}\right] + \left[\frac{k_p-3/2}{k}\frac{2k_pT_{\perp O^+}}{m_{O^+}}\right] \quad (12)$$

$$V^2_{T\Pi l} = \left[\frac{k_p-3/2}{k_p}\frac{2k_pT_{\Pi H^+}}{m_{H^+}}\right] + \left[\frac{k_p-3/2}{k_p}\frac{2k_pT_{\Pi He^+}}{m_{He^+}}\right] + \left[\frac{k_p-3/2}{k_p}\frac{2k_pT_{\Pi O^+}}{m_{O^+}}\right] \quad (13)$$

The kappa distribution function is represented as

$$Z_k(\xi) = \frac{1}{\pi^{1/2}\, {k_p}^{1/2}} \frac{\Gamma(k_p+1)}{\Gamma(k_p-1/2)} \int_{-\infty}^{\infty} \frac{\left(1+\frac{x^2}{k_p}\right)^{-k_p} dx}{(x-\xi)} \quad (14)$$

$$\xi = \frac{(\omega - \Omega_l)}{K_\Pi V_{T\Pi l}}$$

In cases where the perpendicular temperature exceeds the parallel temperature (A>1), free energy stored in this anisotropy can drive wave instabilities, leading to the amplification of EMIC waves. The condition for instability is typically expressed as:

$$\frac{T\perp}{T\parallel} = 1 + \frac{\omega}{\Omega i}$$

https://doi.org/10.5194/angeo-2024-25
Preprint. Discussion started: 20 November 2024

As reported in the study by Gary and Wang (1996),Temperature anisotropy significantly impacts the growth rate and modifies the dispersion properties of electromagnetic ion cyclotron (EMIC) waves. The difference between perpendicular and parallel temperatures in the plasma introduces a source of free energy, which can either enhance or suppress wave propagation. When the anisotropy is sufficiently large, it can destabilize certain wave modes, causing them to grow under specific conditions.

DISPERSION RELATION

Considering the cold plasma dispersion relation for EMIC waves

$$\frac{c^2 k_{\Pi}^2}{\omega^2} = \left(\frac{\omega_{pH^+}^2}{\Omega_{H^+}^2}\right)\left(1-\frac{\omega}{\Omega_{H^+}}\right)^{-1} + \left(\frac{\omega_{pHe^+}^2}{\Omega_{He^+}^2}\right)\left(1-\frac{\omega}{\Omega_{He^+}}\right)^{-1} + \left(\frac{\omega_{pO^+}^2}{\Omega_{O^+}^2}\right)\left(1-\frac{\omega}{\Omega_{O^+}}\right)^{-1} \qquad (15)$$

Where $\omega_{pl}^2 = \frac{4\pi N_l e^2}{m_l}$

This establishes the squared plasma frequency for the ions, while Ωl represents the cyclotron frequency of the respective multi-ion species,

The dispersion relation for an ion electromagnetic cyclotron wave propagating along the direction of an external magnetic field in a system consisting of ions, electrons, and non-ionized particles—including both resonant and non-resonant particles involved in electrical and wave transmission—is described by the dispersion ratio of cold plasma is also close to the dispersion ratio of hot plasma[Error! Reference source not found.]. provided that plasma ck/ω >> 1

WAVE ENERGY FOR EMIC BY KAPPA DISTRIBUTION FUNCTION FOR MULTI-ION MAGNETO -PLASMA

The perpendicular resonant energy and parallel resonant energy are calculated by basic equation of wave energy per unit wavelengths(*Rana et.al 2021*)

so perpendicular resonant energy for ions H^+, He^+ and O^+ is

$$W_{r\perp l} = \frac{\pi^{\frac{3}{2}} B^2}{C^2 K_{\Pi}^2 \omega}\left[\frac{\Gamma(k_p+1)}{k_p^{\frac{3}{2}}\Gamma\left(k_p-\frac{1}{2}\right)V_{T\Pi H^+}^2}\,\omega_{pH^+}^2\,\frac{T_\perp}{T_\Pi}\left(\frac{\omega-\Omega_{H^+}}{\Omega_{H^+}}\right)+1\right]\left[1+\frac{\left(\omega-\Omega_{H^+}\right)^2}{K_{\Pi}^2 V_{T\Pi H^+}^2}\right]^{-k_p-1} +$$

$$\frac{\pi^{3/2} B^2}{C^2 K_{\Pi}^2 \omega}\left[\frac{\Gamma(k_p+1)}{k_p^{3/2}\Gamma(k_p-1/2)V_{T\Pi He^+}^2}\,\omega_{pHe^+}^2\,\frac{T_\perp}{T_\Pi}\left(\frac{\omega-\Omega_{He^+}}{\Omega_{He^+}}\right)+1\right]\left[1+\frac{\left(\omega-\Omega_{He^+}\right)^2}{K_{\Pi}^2 V_{T\Pi He^+}^2}\right]^{-k_p-1} +$$

$$\frac{\pi^{3/2} B^2}{C^2 K_{\Pi}^2 \omega}\left[\frac{\Gamma(k_p+1)}{k_p^{3/2}\Gamma(k_p-1/2)V_{T\Pi O^+}^2}\,\omega_{pO^+}^2\,\frac{T_\perp}{T_\Pi}\left(\frac{\omega-\Omega_{O^+}}{\Omega_{O^+}}\right)+1\right]\left[1+\frac{\left(\omega-\Omega_{O^+}\right)^2}{K_{\Pi}^2 V_{T\Pi O^+}^2}\right]^{-k_p-1} \qquad (16)$$

https://doi.org/10.5194/angeo-2024-25
Preprint. Discussion started: 20 November 2024

And **Parallel resonant energy** is

$$W_{r\Pi l}=\frac{\pi^{3/2}B^2}{C^2K_\Pi^2\omega}\left[\frac{\Gamma(k_p+1)}{k_p{}^{3/2}\Gamma(k_p-1/2)V_{T\Pi H^+}^2}\omega_{pH^+}^2\frac{T_{\perp l}}{T_{\Pi l}}\left(\frac{\omega-\Omega_{H^+}}{\Omega_{H^+}}\right)^2\right]\left[1+\frac{(\omega-\Omega_{H^+})^2}{K_\Pi^2V_{T\Pi H^+}^2}\right]^{-k_p-1}+$$

$$\frac{\pi^{3/2}B^2}{C^2K_\Pi^2\omega}\left[\frac{\Gamma(k_p+1)}{k_p{}^{3/2}\Gamma(k_p-1/2)V_{T\Pi He^+}^2}\omega_{pHe^+}^2\frac{T_{\perp l}}{T_{\Pi l}}\left(\frac{\omega-\Omega_{He^+}}{\Omega_{He^+}}\right)^2\right]\left[1+\frac{(\omega-\Omega_{He^+})^2}{K_\Pi^2V_{T\Pi He^+}^2}\right]^{-k_p-1}+$$

$$\frac{\pi^{3/2}B^2}{C^2K_\Pi^2\omega}\left[\frac{\Gamma(k_p+1)}{k_p{}^{3/2}\Gamma(k_p-1/2)V_{T\Pi O^+}^2}\omega_{pO^+}^2\frac{T_{\perp l}}{T_{\Pi l}}\left(\frac{\omega-\Omega_{O^+}}{\Omega_{O^+}}\right)^2\right]\left[1+\frac{(\omega-\Omega_{O^+})^2}{K_\Pi^2V_{T\Pi O^+}^2}\right]^{-k_p-1} \qquad (17)$$

GROWTH RATE

the k-Lorentz distribution impacts the growth rate of electromagnetic waves in a plasma by changing the effective plasma density and modifying the dispersion relations due to its non-thermal characteristics. This leads to differences in wave behaviour compared to what is predicted by a Maxwellian distribution[Error! Reference source not found.].

By applying the law of conservation of energy, the growth rate can be determined as follows:

$$\frac{\gamma}{\omega_l}=\frac{\frac{\pi^{3/2}\Omega_{H^+}}{K_\Pi V_{T\Pi H^+}}\left[\frac{\Gamma(k_p+1)}{k_p{}^{3/2}\Gamma(k_p-1/2)}\left(1-\frac{\omega}{\Omega_{H^+}}\right)\left(\frac{T_{\perp H^+}}{T_{\Pi H^+}}\right)-1\right]\times\left[1+\frac{\left(\omega-\Omega_{H^+}\right)^2}{K_\Pi^2V_{T\Pi H^+}^2}\right]^{-k_p-1}}{\left(\frac{CK_\Pi}{\omega_{pH^+}^2}\right)^2\left(\frac{2\Omega_{H^+}-\omega}{\Omega_{H^+}-\omega}\right)+\frac{1}{2}\frac{\omega^2}{\left(\Omega_{H^+}-\omega\right)^2}}+$$

$$\frac{\frac{\pi^{3/2}\Omega_{He^+}}{K_\Pi V_{T\Pi He^+}}\left[\frac{\Gamma(k_p+1)}{k_p{}^{3/2}\Gamma(k_p-1/2)}\left(1-\frac{\omega}{\Omega_{He^+}}\right)\left(\frac{T_{\perp He^+}}{T_{\Pi He^+}}\right)-1\right]\times\left[1+\frac{\left(\omega-\Omega_{He^+}\right)^2}{K_\Pi^2V_{T\Pi He^+}^2}\right]^{-k_p-1}}{\left(\frac{CK_\Pi}{\omega_{pHe^+}^2}\right)^2\left(\frac{2\Omega_{He^+}-\omega}{\Omega_{He^+}-\omega}\right)+\frac{1}{2}\frac{\omega^2}{\left(\Omega_{He^+}-\omega\right)^2}}+$$

$$\frac{\frac{\pi^{3/2}\Omega_{O^+}}{K_\Pi V_{T\Pi O^+}}\left[\frac{\Gamma(k_p+1)}{k_p{}^{3/2}\Gamma(k_p-1/2)}\left(1-\frac{\omega}{\Omega_{O^+}}\right)\left(\frac{T_{\perp O^+}}{T_{\Pi O^+}}\right)-1\right]\times\left[1+\frac{\left(\omega-\Omega_{O^+}\right)^2}{K_\Pi^2V_{T\Pi O^+}^2}\right]^{-k_p-1}}{\left(\frac{CK_\Pi}{\omega_{pO^+}^2}\right)^2\left(\frac{2\Omega_{O^+}-\omega}{\Omega_{O^+}-\omega}\right)+\frac{1}{2}\frac{\omega^2}{\left(\Omega_{O^+}-\omega\right)^2}} \qquad (18)$$

GROWTH LENGTH

The growth length of the electromagnetic ion cyclotron wave is derived fromError! Reference source not found.

$$\boldsymbol{L_g}=\frac{\boldsymbol{V_{gl}}}{\boldsymbol{\gamma}}$$

Where, $\boldsymbol{\gamma}$ is growth rate, $\boldsymbol{V_{gl}}$ is group velocity of the wave

https://doi.org/10.5194/angeo-2024-25
Preprint. Discussion started: 20 November 2024

So now

$$L_g = \frac{1}{\gamma\omega_{pH^+}^2}\left(-C^2K_\Pi\Omega_{H^+} + \frac{C^4K_\Pi^3+2C^2\omega_{pH^+}^2+K_\Pi\Omega_{H^+}}{\sqrt{C^4K_\Pi^4+4C^2\omega_{pH^+}^2+K_\Pi^2\Omega_{H^+}}}\right) + \frac{1}{\gamma\omega_{pHe^+}^2}\left(-C^2K_\Pi\Omega_{He^+} + \frac{C^4K_\Pi^3+2C^2\omega_{pHe^+}^2+K_\Pi\Omega_{He^+}}{\sqrt{C^4K_\Pi^4+4C^2\omega_{pHe^+}^2+K_\Pi^2\Omega_{He^+}}}\right) + \frac{1}{\gamma\omega_{pO^+}^2}\left(-C^2K_\Pi\Omega_{O^+} + \frac{C^4K_\Pi^3+2C^2\omega_{pO^+}^2+K_\Pi\Omega_{O^+}}{\sqrt{C^4K_\Pi^4+4C^2\omega_{pO^+}^2+K_\Pi^2\Omega_{O^+}}}\right) \quad (19)$$

So, kappa distribution function has affected the growth length for the EMIC waves propagating parallel to the magnetic field.

RESULT AND DISCUSSION:-

The results show the impact of different kappa distribution indices on the characteristics of EMIC waves. The study provides analytical expressions for various parameters, helping to understand the behaviour of these waves in different plasma conditions. The following plasma parameters, relevant to the auroral acceleration region, are used for the numerical evaluation of the dispersion relation, resonant energies, growth rate and Growth length with the steepness of kappa distribution functionError! Reference source not found.

B_O=4300nT $\quad \Omega_{H^+} = 412S^{-1} \quad \Omega_{He^+} = 102.5S^{-1}$

$\Omega_{O^+} = 25.625S^{-1}\ \frac{V_{T\perp e}^2}{V_{T\Pi e}} = .10-02$

$\omega_{pH^+}^2 = 1.248\times10^7S^{-2} \quad \omega_{pHe^+}^2 = 1.147\times10^6S^{-2} \ \omega_{pO^+}^2 = 7.348\times10^5S^{-2}$

$V_{T\Pi o} = 5\times10^7S^{-2} \qquad V_{T\Pi h} = 2\times10^8S^{-2} \ V_{T\Pi he} = 6\times10^7S^{-2}$

The equation 15,16,17,18 and 19 is evaluated using Mathcad software to solve for resonant energies, growth rates, and growth lengths.

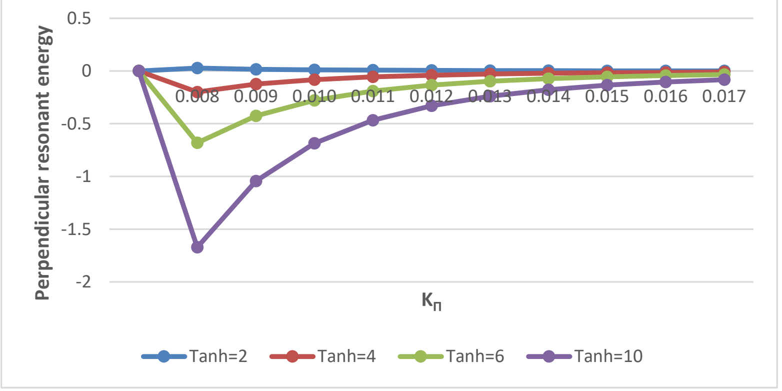

Fig. 1 Variation of the perpendicular resonant energy $W_\perp$ erg cm^{-1}versus the wave vector $\mathbf{K_\Pi}$ (cm^{-1}) for varying values of the Hydrogen ion Temperature Anisotropy at κ_p=2 .

https://doi.org/10.5194/angeo-2024-25
Preprint. Discussion started: 20 November 2024

The curves 1 demonstrate how the system's resonant energy responds to different levels of temperature anisotropy (Tanh = 2, 4, 6, and 10) as κ_π increases. Across all curves, there is an eventual stabilization of the resonant energy, but the effect varies significantly depending on the anisotropy level.

High Anisotropy: Strongly impacts the system by significantly lowering the resonant energy at low κ_π , followed by a gradual recovery as κ_π increases.

Moderate Anisotropy: Shows a smaller dip in energy, with the system stabilizing more quickly as κ_π increases, indicating a moderate influence.

Low Anisotropy: Exhibits stable resonant energy, with minimal response to changes in κ_π, meaning anisotropy has a limited effect on the system at these levels.

Temperature anisotropy has a significant role in determining the perpendicular resonant energy, particularly in systems with higher anisotropy. At high anisotropy levels, the system experiences a notable suppression of energy that recovers as κ_π increases. In contrast, lower anisotropy causes only minor fluctuations in energy, showing the system is more resilient to changes in κ_π when anisotropy is low.

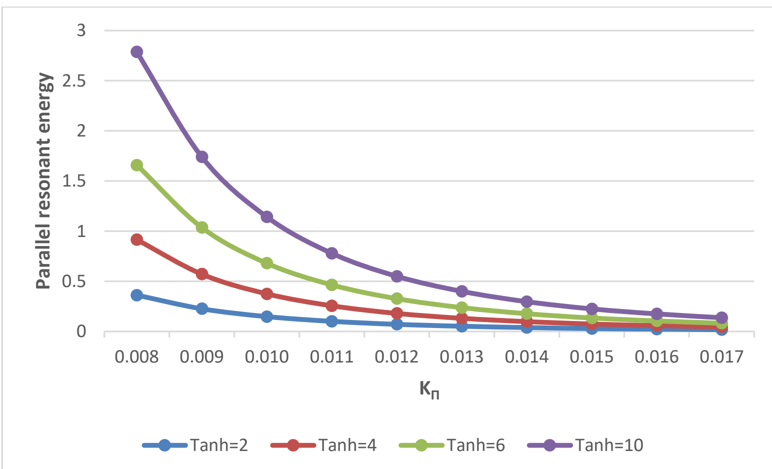

Fig. 2 Variation of parallel resonant energy W_{II} erg cm^{-1} versus wave vector $\mathbf{K_{II}}$ (cm^{-1}) for varying values of the Hydrogen ion Temperature Anisotropy at κ_p=2 .

This graph 2 shows the behavior of parallel resonant energy as a function of κ_π for different levels of temperature anisotropy (Tanh = 2, 4, 6, and 10). The curves demonstrate that as κ_π increases, the parallel resonant energy decreases, with the effect being stronger for higher anisotropy values.

https://doi.org/10.5194/angeo-2024-25
Preprint. Discussion started: 20 November 2024

- High Anisotropy (Tanh = 10): The energy starts high (~3) and decreases rapidly as κ_π increases, indicating that a highly anisotropic system has more energetic particles, but this energy reduces as κπ grows.
- Moderate Anisotropy (Tanh = 6): The energy starts at a lower value (~1.5) and follows a similar decreasing trend, though it stabilizes faster than at higher anisotropies.
- Low Anisotropy (Tanh = 2, 4): For these lower anisotropy values, the energy starts smaller and decreases more gradually, indicating a more stable system that is less affected by changes in κ_π .

The parallel resonant energy is strongly influenced by temperature anisotropy. At high anisotropy (Tanh = 10), the system initially has a large parallel energy, which decays rapidly as κ_π increases, reflecting the diminishing influence of suprathermal particles in the kappa distribution. In contrast, at lower anisotropies (Tanh = 2, 4), the system is closer to thermal equilibrium, and the parallel resonant energy remains more stable. This graph highlights the interplay between κ_π and anisotropy, with anisotropy having a more pronounced effect on the parallel resonant energy in highly non-thermal regimes.

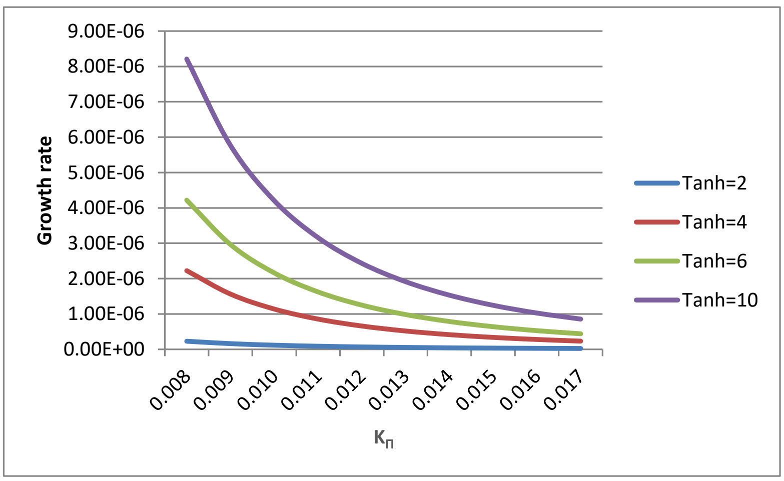

Fig. 3 Variation of growth rate (γ/ω) versus wave vector $\mathbf{K_{II}}$ (cm^{-1}) for varying values of the Hydrogen ion Temperature Anisotropy at κ_p=2

The graph shows that growth rate decreases as κ_π increases for different temperature anisotropies (Tanh = 2, 4, 6, 10).

- **High Anisotropy (Tanh = 10)**: Highest initial growth rate, decaying rapidly with increasing κ_π , indicating strong initial plasma instability.

https://doi.org/10.5194/angeo-2024-25
Preprint. Discussion started: 20 November 2024

- **Moderate Anisotropy (Tanh = 6, 4)**: Lower initial growth rates, with more gradual decay, showing less instability compared to higher anisotropy.
- **Low Anisotropy (Tanh = 2)**: Minimal growth rate, suggesting near stability from the start.

plasma growth rate, temperature anisotropy, and the kappa distribution, showing how higher anisotropy amplifies growth rates but quickly stabilizes as the system moves toward a more thermal state with higher κ_π.

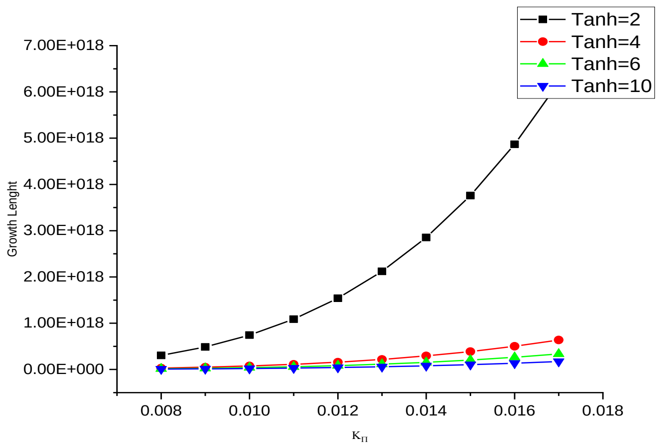

Fig. 4 Variation of growth length Lg versus wave vector $\mathbf{K_{II}}$ (cm^{-1}) for varying values of the Hydrogen ion Temperature Anisotropy at κ_p=2

The graph 4 indicates that as the wave vector increases, the growth length becomes larger, implying that shorter wavelength waves experience faster growth or stronger instability. The temperature anisotropy (Tanh), which reflects differences in temperature along different directions in the plasma, plays a secondary role in modulating the growth length. While its influence is more apparent at higher wave vectors, the dominant factor driving the growth length is the wave vector itself. Temperature anisotropy adds a secondary effect, especially at high wave vectors, where higher anisotropy (Tanh = 10) leads to slightly larger growth lengths compared to lower anisotropies.

https://doi.org/10.5194/angeo-2024-25
Preprint. Discussion started: 20 November 2024

Annales Geophysicae Discussions Open Access EGU

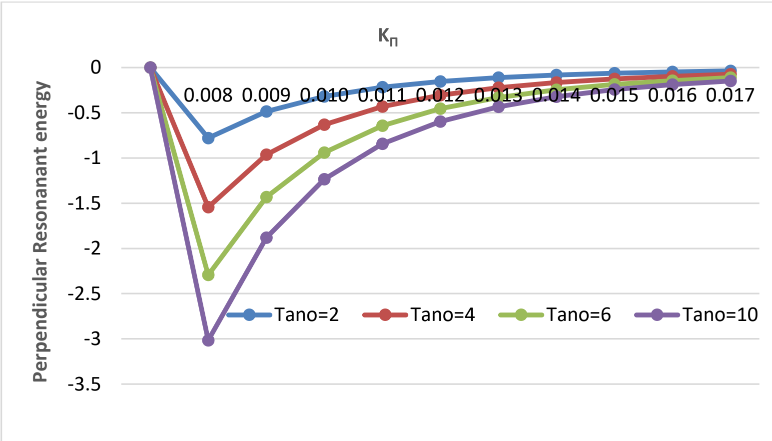

Fig. 5 Variation of the perpendicular resonant energy $W_{\perp}$ erg cm^{-1}versus the wave vector $\mathbf{K_{II}}$ (cm^{-1}) for varying values of the Oxygen ion Temperature Anisotropy at κ_p=2

In figure 5 In the context of oxygen ions, the temperature anisotropy refers to the difference between the temperature in The directions parallel and perpendicular relative to the magnetic field. The sharp decrease in resonant energy with increasing κ_π, followed by a recovery, could imply a dynamic interaction between ions and magnetic fields. Higher anisotropy seems to enhance energy loss at lower κ_π , but this effect diminishes as κ_π increases.this graph highlights how perpendicular resonant energy is influenced by both the temperature anisotropy and the parameter κ_π . Higher temperature anisotropy results in a more pronounced initial energy loss, but the energy converges to similar values for all anisotropies as κ_π increases.

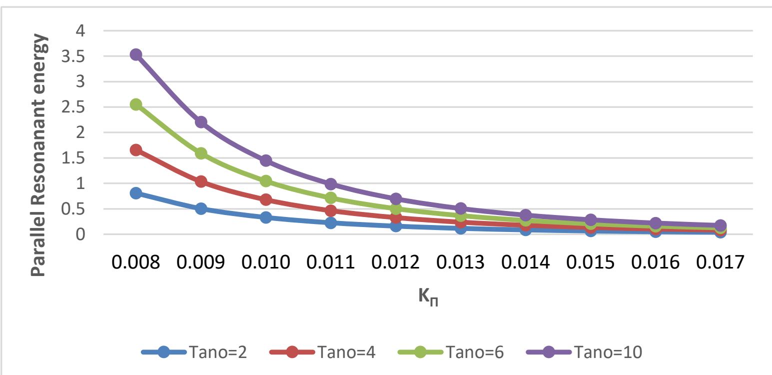

Fig. 6 Variation of parallel resonant energy W_{II} erg cm^{-1} versus wave vector $\mathbf{K_{II}}$ (cm^{-1}) for varying values of the Oxygen ion Temperature Anisotropy at κ_p=2 .

https://doi.org/10.5194/angeo-2024-25
Preprint. Discussion started: 20 November 2024

In figure 6 graph, the oxygen temperature anisotropy influences the behavior of parallel resonant energy similarly to how it affects perpendicular resonant energy. The larger the temperature anisotropy, the more pronounced the initial parallel resonant energy. However, as κ_π increases, the resonant energy decreases for all Tano values, indicating that higher values of κ_π diminish the energy differences caused by anisotropy.The sharper drop in parallel resonant energy for higher Tano values reflects the increased energy loss due to stronger anisotropy at lower κ_π . The gradual convergence of all curves at higher κ_π suggests that for large enough κ_π, anisotropy becomes less important in determining the parallel resonant energy.

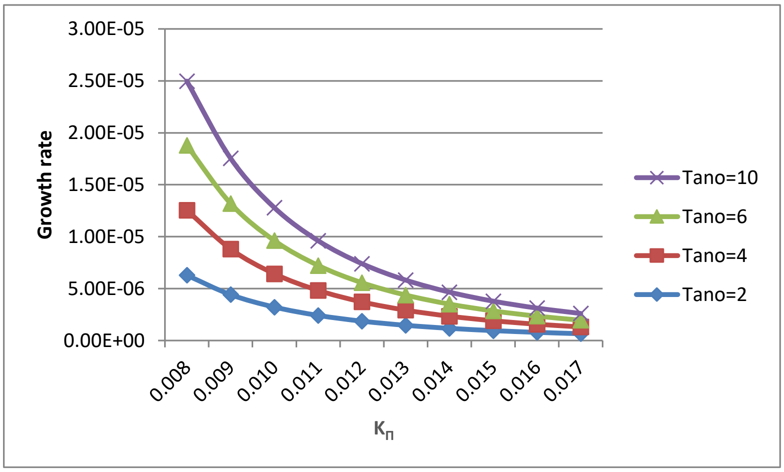

Fig. 7 Variation of growth rate (γ/ω) versus wave vector $\mathbf{K_{II}}$ (cm^{-1}) for varying values of the Oxygen ion Temperature Anisotropy at κ_p=2

In figure 7 graph For lower values of κ_π the difference in growth rates among different Temperature anisotropy in oxygen values is more pronounced, with Tano = 10 being significantly higher.As κ_π increases, the growth rates converge, and the differences between Temperature anisotropy values become less noticeable.: Higher Temperature anisotropy in oxygen values (representing some physical or operational parameter) lead to higher growth rates initially, but all curves eventually decline towards zero as κ_π increases, suggesting a diminishing effect of κ_π on growth rate regardless of Tano.

https://doi.org/10.5194/angeo-2024-25
Preprint. Discussion started: 20 November 2024

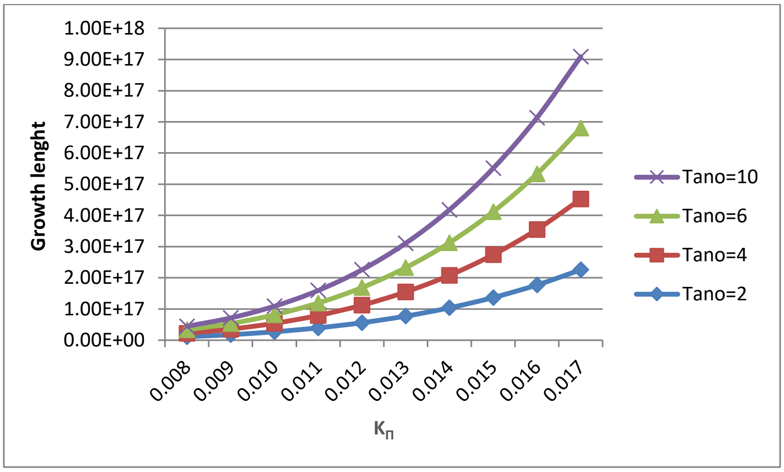

Fig. 8 Variation of growth length Lg versus wave vector **K** K_{II} (cm^{-1})for varying values of the Oxygen ion Temperature Anisotropy at κ_p=2

The graph 8 likely represents how growth length increases as κ_π increases. Temperature anisotropy in oxygen plays a critical role in determining how fast or slow this growth occurs. Growth length increases exponentially with κ_π, and this effect is amplified by higher temperature anisotropy. Higher anisotropy values lead to a more rapid rise in growth length, especially at higher κ_π .The effect of anisotropy is more pronounced at higher values of κ_π, where the curves diverge significantly, showing that anisotropy strongly influences growth processes in such conditions.

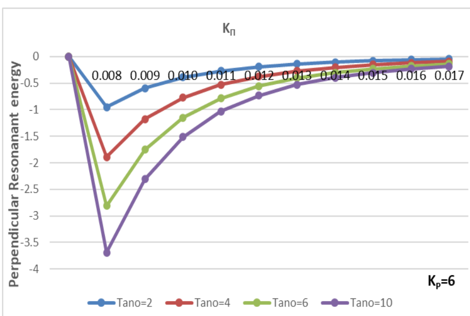

Fig. 9 Variation of the perpendicular resonant energy $W_\perp$ erg cm^{-1}versus the wave vector **K_{II}** (cm^{-1}) for varying values of the Oxygen ion Temperature Anisotropy at κ_p=6

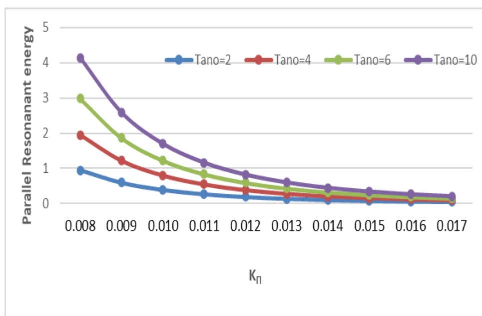

Fig. 10 Variation of parallel resonant energy W_{II} erg cm^{-1} versus wave vector **K_{II}** (cm^{-1}) for varying values of the Oxygen ion Temperature Anisotropy at κ_p=6 .

https://doi.org/10.5194/angeo-2024-25
Preprint. Discussion started: 20 November 2024

In figure 9 and 10 graph The perpendicular energy experiences a steep decline at the lowest κ_π values, particularly for higher Tano values, before gradually increasing towards zero as κ_π rises. This indicates a strong initial impact of anisotropy that diminishes with increasing κ_π.In contrast, the parallel resonant energy starts high and decreases steadily with κ_π. Higher Tano levels result in higher initial energy values, but similar to the perpendicular energy, all values converge towards zero as κ_π increases. The analysis reveals that oxygen temperature anisotropy significantly alters resonant energy states at low κ_π , enhancing both perpendicular and parallel energies in different ways. However, as κ_π increases, the system stabilizes, and the influence of anisotropy diminishes, leading to near-uniform energy levels regardless of the anisotropy magnitude. This behaviour highlights the complex interplay between anisotropy and κ_π in shaping energy dynamics

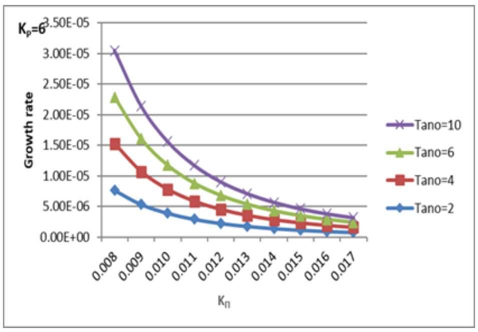

Fig. 11 Variation of growth rate (γ/ω) versus wave vector KII (cm-1) for varying values of the Oxygen ion Temperature Anisotropy at κp=6

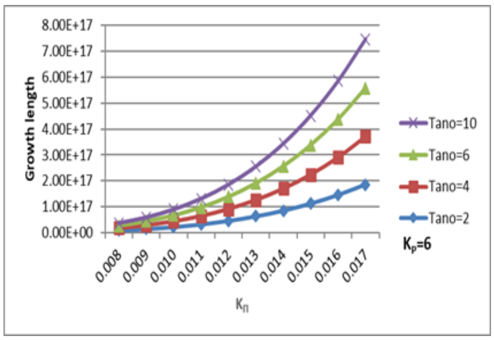

Fig. 12 Variation of growth length Lg versus wave vector **K**$_{II}$ (cm^{-1}) for varying values of the Oxygen ion Temperature Anisotropy at κ_p=6

The two graphs 11 and 12 illustrate the influence of temperature anisotropy (Tano) on growth rate and growth length as functions of κ_π, with a fixed $\kappa_p = 6$. In the 11 graphs, showing the growth rate versus κ_π, a clear trend emerges where the growth rate decreases as κ_π increases, regardless of the Tano value. Higher Tano values, such as Tano=10, lead to significantly higher growth rates compared to lower values like Tano=2. This indicates that temperature anisotropy enhances the growth rate, particularly at lower κ_π values. However, as κ_π increases, the growth rates of different Tano levels converge, suggesting that the impact of Tano diminishes at higher κ_π values.

In the 12 graph, which depicts growth length versus κ_π, the opposite trend is observed: growth length increases with κ_π for all Tano values. Higher Tano values correspond to much

https://doi.org/10.5194/angeo-2024-25
Preprint. Discussion started: 20 November 2024

larger growth lengths, emphasizing the strong effect of temperature anisotropy on this metric. The separation between the growth length curves becomes more pronounced as κ_π increases, with higher Tano values resulting in significantly greater growth lengths. This suggests that while the impact of Tano on growth rate lessens with increasing κ_π, its influence on growth length remains substantial.

Overall, the combined analysis highlights the critical role of temperature anisotropy in determining growth dynamics. Higher Tano values enhance both growth rate and growth length. This interplay suggests that while κ_p inversely affects growth rate and positively influences growth length, the extent of these effects is strongly modulated by the degree of temperature anisotropy.

CONCLUSION:

This study has explored the impact of temperature anisotropy and the Kappa distribution function on the propagation and characteristics of electromagnetic ion cyclotron (EMIC) waves in a multi-ion magneto-plasma environment. By incorporating the effects of anisotropic thermal conditions and non-Maxwellian particle distributions, the research provides a deeper understanding of how these factors alter wave dynamics, including dispersion relations, growth rates, and energy states. Our findings reveal significant deviations from classical models, emphasizing the necessity to account for both temperature anisotropy and suprathermal particles for accurate modeling of wave behavior in realistic space and laboratory plasmas.

The results demonstrate that high levels of temperature anisotropy lead to notable changes in wave characteristics, such as enhanced growth rates and altered resonant energy patterns. As the Kappa distribution index increases, these effects tend to diminish, indicating that the influence of anisotropy becomes less pronounced in more thermalized systems. This nuanced interaction between anisotropy and the Kappa distribution highlights the complexity of plasma wave dynamics, especially in environments like the Earth's magnetosphere and other astrophysical contexts where multi-ion interactions and non-equilibrium conditions prevail.

Overall, this study enhances the overall comprehension of space plasma physics and has potential applications in predicting wave behavior in the Earth's magnetosphere, astrophysical plasma conditions, and controlled plasma experiments. Future research should explore these interactions under varying magnetic field strengths and other plasma parameters to further refine theoretical models and enhance the predictive capabilities for space weather phenomena.

Competing interests

The contact author has declared that none of the authors has any competing interests.

Reference

1. Meda, R., and Ahirwar, G.: Investigating electromagnetic ion cyclotron wave propagation in multi-ion plasmas, *JETIR*, **8**(8), 1–6, 2021.
2. Ahirwar, G., Varma, P., and Tiwari, M. S.: Ion cyclotron resonance in magnetospheric plasmas, *Indian J. Pure Appl. Phys.*, **48**, 334–342, 2010.
3. Ahirwar, G., Varma, P., and Tiwari, M. S.: Electromagnetic wave propagation in magnetospheric plasmas, *Indian J. Phys.*, **80**, 1179–1187, 2006.
4. Anderson, B. J., and Williams, D. J.: The electromagnetic ion cyclotron wave and its interaction with the magnetosphere, *Space Sci. Rev.*, **89**(1–2), 253–268, 1999.
5. Chen, L. J., and Hasegawa, A.: The influence of temperature anisotropy on the properties of EMIC waves, *J. Geophys. Res.*, **79**(19), 2894–2904, 1974.
6. Del Sarto, D., Pegoraro, F., and D'Angelo, R.: Wave propagation in non-Maxwellian plasmas, *Phys. Plasmas*, **18**(10), 102104, 2011.
7. Hellinger, P., and Matsumoto, Y.: The effect of temperature anisotropy on ion cyclotron waves in a multi-ion plasma, *J. Geophys. Res.*, **105**(A10), 23139–23148, 2000.
8. Kennel, C. F., and Petschek, H. E.: Limit on stably trapped particle fluxes, *J. Geophys. Res.*, **71**(1), 1–28, 1966.
9. Pierrard, V., and Lazar, M.: Kappa distributions: A review, *Nonlinear Process. Geophys.*, **17**(3), 209–220, 2010.
10. Scholer, M.: The effect of temperature anisotropy on the growth of electromagnetic ion cyclotron waves, *J. Geophys. Res.*, **93**(A8), 8753–8764, 1988.
11. Vasyliunas, V. M.: Theoretical models of magnetospheric convection, *J. Geophys. Res.*, **73**(21), 7466–7481, 1968.
12. Zhang, J., and Chen, L.: Temperature anisotropy effects on the stability of ion cyclotron waves, *Phys. Plasmas*, **10**(4), 1148–1156, 2003.
13. Ahirwar, G., Varma, P., and Tiwari, M. S.: Ion cyclotron instability in magnetospheric plasmas, *Ann. Geophys.*, **24**, 1919–1932, 2006.

https://doi.org/10.5194/angeo-2024-25
Preprint. Discussion started: 20 November 2024

14. Meda, R., and Ahirwar, G.: Study of EMIC waves in space plasmas, *Int. J. Sci. Dev. Res.*, **7**(9), 1–7, 2022.
15. Sharma, J., and Ahirwar, G.: Study on EMIC waves in multi-ions around the plasmapause region, *Res. J. Phys. Sci.*, **1**(3), 26–29, 2013.
16. Summers, D., and Thorne, R. M.: Electromagnetic ion cyclotron instability in space plasmas, *J. Geophys. Res.*, **108**(A4), 1143, https://doi.org/10.1029/2002JA009489, 2003.
17. Gamayunov, K. V., Khazanov, G. V., Liemohn, M. W., Fok, M. C., and Ridley, A. J.: Self-consistent magnetosphere-ionosphere coupling model, *J. Geophys. Res.: Space Phys.*, **114**, A03221, 2009.
18. Kennel, C. F., and Petschek, H. E.: Limit on stably trapped particle fluxes, *J. Geophys. Res.*, **71**(1), 1–28, 1966.
19. Erlandson, R. E., and Ukhorskiy, A. Y.: Interactions between electromagnetic ion cyclotron waves and ring current ions, *J. Geophys. Res.: Space Phys.*, **106**(A5), 3883–3890, 2001.
20. Anderson, B. J., Erlandson, R. E., and Zanetti, L. J.: A statistical study of Pc 1-2 magnetic pulsations in the equatorial magnetosphere: 1. Equatorial occurrence distributions, *J. Geophys. Res.: Space Phys.*, **97**(A3), 3075–3088, 1992.
21. Gurgiolo, C., Sandel, B. R., Perez, J. D., Mitchell, D. G., Pollock, C. J., and Larsen, B. A.: MHD waves in the outer magnetosphere, *J. Geophys. Res.: Space Phys.*, **110**, A12217, 2005.
22. Mozer, F. S., Carlson, C. W., and Hudson, M. K.: Electromagnetic ion cyclotron waves and their interactions with the magnetosphere, *Phys. Rev. Lett.*, **38**(6), 292–295, 1977.
23. Temerin, M., Cerny, K., Lotko, W., and Mozer, F. S.: The role of Alfvén waves in auroral particle acceleration, *Phys. Rev. Lett.*, **48**(18), 1175–1178, 1982.
24. Song, Y., and Lysak, R. L.: Alfvén waves and their role in the magnetosphere-ionosphere coupling, *Phys. Rev. Lett.*, **96**, 145002, 2006.
25. Lund, E. J., Mobius, E., Carlson, C. W., et al.: Investigating wave propagation and reflection in the magnetosphere, *J. Atmos. Solar-Terr. Phys.*, **62**(4), 467–476, 2000.
26. Khazanov, G. V., Gamayunov, K. V., Gallagher, D. L., and Kozyra, J. U.: Electromagnetic ion cyclotron waves and their effects in the magnetosphere, *J. Geophys. Res.: Space Phys.*, **111**, A10202, https://doi.org/10.1029/2006JA011833, 2006.

https://doi.org/10.5194/angeo-2024-25
Preprint. Discussion started: 20 November 2024

Annales Geophysicae Discussions

27. Lund, E. J., Mobius, E., Klumpar, D. M., et al.: Observations of plasma wave activity in the Earth's magnetosphere, *Adv. Space Res.*, **23**(10), 1721–1726, 1999.

28. Varma, P., Ahirwar, G., and Tiwari, M. S.: Electromagnetic ion cyclotron waves and their interaction with multi-ion plasmas, *Planet. Space Sci.*, **56**(8), 1023–1031, 2008.

29. Vasyliunas, V. M.: A survey of low-energy electrons in the evening sector of the magnetosphere with OGO 1 and OGO 3, *J. Geophys. Res.*, **73**(9), 2839–2884, https://doi.org/10.1029/JA073i009p02839, 1968.

30. Pierrard, V., and Lazar, M.: Kappa distributions: Theory and applications in space plasmas, *Solar Phys.*, **267**(1), 153–174, https://doi.org/10.1007/s11207-010-9640-2, 2010.

31. Gary, S. P., and Lee, M. A.: The ion cyclotron anisotropy instability and the inverse correlation between proton anisotropy and proton beta, *J. Geophys. Res.: Space Phys.*, **99**(A6), 11297–11302, https://doi.org/10.1029/94JA00253, 1994.

32. Hellinger, P., Trávníček, P. M., Kasper, J. C., and Lazarus, A. J.: Solar wind proton temperature anisotropy: Linear theory and WIND/SWE observations, *Geophys. Res. Lett.*, **33**(9), https://doi.org/10.1029/2006GL025925, 2006.

33. Baumjohann, W., and Treumann, R. A.: Basic Space Plasma Physics, Imperial College Press, 1997.

34. Schindler, K.: Physics of Space Plasma Activity, Cambridge University Press, 2007.

35. Cornwall, J. M., and Schulz, M.: Theoretical investigation of ion cyclotron resonance, *J.